

Angular resolution of the MIMAC Dark Matter directional detector

Y. Tao,^{a,1} I. Moric,^a C. Tao,^{c,a} D. Santos,^b N. Sauzet,^b C.
Couturier,^b O. Guillaudin,^b J.F. Muraz,^b F. Naraghi,^b N. Zhou^{d,a}
and J. Busto^c

^aTsinghua Center for Astrophysics, Department of Physics, Tsinghua University,
Beijing 100084, China

^bLaboratoire de Physique Subatomique et de Cosmologie, Universit Grenoble-Alpes(UGA),
CNRS/IN2P3, Institut Polytechnique de Grenoble,
53, rue des Martyrs, Grenoble, France

^cCentre de Physique des Particules de Marseille, Aix-Marseille Université, CNRS/IN2P3,
Marseille, France

^dINPAC and School of Physics and Astronomy, Shanghai Jiao Tong University, Shanghai
Laboratory for Particle Physics and Cosmology,
Shanghai 200240, China

E-mail: taoy15@mails.tsinghua.edu.cn

Abstract. Dark Matter (DM) in the form of Weakly Interacting Massive Particles (WIMPs) has been searched for since the 1980's. WIMPs interact with nuclei of the detectors. If a signal is observed in direct detection experiments, the best signature for its Galactic origin would be with a directional detector [1]. To meet that challenge, directional Dark Matter detectors should be sensitive to low energy recoils in the keV range and have an angular resolution better than 20° [2]. MIMAC (MIcro-TPC MAtrix of Chambers) is a low pressure gas detector which provides both the kinetic energy and three-dimensional track reconstruction of electron and ion tracks. We use specially developed low energy (1-25 keV) ion beam facilities to test the MIMAC response. In this paper we report the first ever observations of ^{19}F ion tracks in this low energy range. We have studied the track lengths (depths), widths and angular spreads with respect to the incoming ion direction. The estimated angular resolution is better than 10° at the measured energies. This is very encouraging for the hope to get a signature of the Galactic origin of a Dark Matter signal.

ArXiv ePrint: [19XX.XXXXX](https://arxiv.org/abs/19XX.XXXXX)

¹Corresponding author.

Contents

| | | |
|----------|---|----------|
| 1 | Introduction | 1 |
| 2 | Experimental setup and low-energy facilities | 2 |
| 2.1 | The MIMAC detector | 2 |
| 2.2 | Low energy beam facilities: COMIMAC and LHI | 3 |
| 2.3 | Experimental conditions | 4 |
| 3 | Track Reconstruction | 4 |
| 3.1 | Track angle, angular resolution, depth and width definitions | 4 |
| 3.2 | Effects on angular resolution | 6 |
| 3.3 | Analysis results on track depth, width and angular resolution | 6 |
| 4 | Simulations and Measurements | 7 |
| 5 | Conclusion | 8 |

1 Introduction

The Dark Matter hypothesis plays a central role in large scale cosmology and galaxy formation. The most widely accepted Dark Matter particle candidate is the Weakly Interacting Massive Particle (WIMP). Since Goodman and Witten [3] have proposed to detect the nuclear recoils produced by WIMP elastic collisions with target nuclei, many Dark Matter detectors have been tested. This paper addresses the performance of the MIMAC (MIcro-TPC MAtrix of Chambers) directional Dark Matter detector, a time projection chamber which gas is at low pressure to allow for the observation of low energy (keV) particles tracks. It provides simultaneous measurements of the energy and direction information of ion tracks, hence providing detection of nuclear recoils from WIMPs interactions at energies down to a few keV.

Spergel [1] has proposed to use a directional Dark Matter detector to demonstrate the Galactic origin of an eventual Dark Matter signal. Couturier et al.[4] have compared how different directional detectors, including anisotropic crystals, nuclear emulsions and low pressure gases preserve the initial direction. The study shows that low pressure TPCs provide the best access to this information. Projects such as DRIFT [5] (USA, UK), DM-TPC [6] at MIT (USA), Newage [7] (Japan) and MIMAC [8] (France-China) are trying to achieve directional detection with different techniques (see [9], [10] or [11] for a review).

While the electron background, produced by γ -rays, and muons can be rejected from the intrinsic response of the detectors, neutrons and neutrino interactions producing a WIMP-like signal require additional discrimination effort. Neutrons in an underground laboratory are produced from interactions of high energy muons on the rock and (α, n) reactions produced by the natural decay of uranium and thorium daughter, in particular ^{222}Rn . While passive shielding and active vetos can be used to reduce the neutron background, there is no shielding or discrimination possibility for the neutrinos. In addition, the neutrino background from the Sun, will produce nuclear recoils in the same energy range in which we expect to find Dark Matter particles. The neutrino floor is the ultimate limit to the performance of non-directional detectors [12].

Taking the example of a 10 kg CF_4 50 m^3 MIMAC detector with a recoil energy range of (5, 50) keV, angular resolution of 10° and after 3 years of operation, Billard et al. [13] conclude from simulations that even in the presence of significant background, the detector could set constraints comparable or better than existing detectors for spin-dependent interactions, published by PICO in 2017 [14]. The analysis is based on comparing the expected WIMP flux anisotropy coming from the direction of the solar velocity vector (Cygnus constellation) to the neutron and neutrino background. A statistical map-based analysis is used to derive both the direction of detected events and their number. It can constrain the WIMP-nucleon cross section and derive the Dark Matter halo distribution, even in the presence of a large background contamination ([15] and [13]). If the WIMP-nucleon cross section is about 10^{-4} pb and the WIMP mass is $100 \text{ GeV}\cdot\text{c}^{-2}$, Dark Matter would be detected with a significance greater than 3σ [15]. Billard et al. [2] show that with a 100% sense recognition, an angular resolution of 20° and with no background contamination, this type of detector could reach a 3σ sensitivity at 90% down to 10^{-5} pb for a WIMP-proton cross section which is spin dependent. In a pessimistic case with an energy threshold of 20 keV, angular resolution of 50° , no sense recognition capability and with a background contamination of 10 event/(kg·yr) the cross section sensitivity would be better than 3×10^{-4} pb.

Within the next decade, we expect that large mass non-directional detectors will either observe a Dark Matter signal, or reach the solar neutrino floor. A directional detector will then be needed to confirm the Galactic origin of the signal, or to improve on the neutrino floor background.

This paper presents the MIMAC detector prototype performance in terms of its angular resolution at low nuclear recoil kinetic energies (6 to 26 keV). The experimental setup consists of a MIMAC chamber prototype connected to an ion beam facility. It is presented in Section 2. Next, in Section 3 we explain how we define and reconstruct the ion track direction, "depths" and "widths" and discuss the angular resolution, measured by the MIMAC detector. We present the exciting results we obtained, a reconstructed angular resolution below 8° at an energy as low as 10 keV!

In Section 4 we compare the measured 3D track depths and widths with SRIM simulations, and note that even if we add the diffusion, there is a large difference for the depths, more than the difference observed on the widths. We discuss the possible origin of the difference between observations and simulations and propose to perform future measurements that will allow us to better understand such discrepancies.

2 Experimental setup and low-energy facilities

2.1 The MIMAC detector

The MIMAC detector is a matrix of micro-Time Projection Chamber (TPC) ([16], [17] and [18]) developed in collaboration between LPSC (Grenoble) and IRFU (Saclay). A chamber of the MIMAC matrix is based on a direct coupling of a pixellized Micromegas with a specially developed fast self-triggered electronics.

The MIMAC gas mixture for dark matter search is 70% CF_4 + 28% CHF_3 + 2% C_4H_{10} at a pressure of 50 mbar. The combination of the gas chosen mixture and pressure provide the necessary conditions for high gain and drift velocity of primary electrons (about $22 \mu\text{m}/\text{ns}$) in the chamber for 3D reconstruction of a few keV nuclear recoil tracks [19]. ^{19}F , being an odd light nucleus represents an interesting target for spin dependent interactions, for which low

pressure Dark Matter gas detectors are still competitive. The gas mixture can be changed to explore other nuclear targets, which is one advantage of a gaseous detector.

The nuclear recoil produced by an eventual elastic WIMP collision, or any ion injected in the detector, releases part of its kinetic energy in the form of ionization. The primary electrons drift under an electric field of 150 V/cm to the grid of a bulk Micromegas [20] producing avalanches under the influence of a high electric field, greater than 10 kV/cm in a thin 512 μm amplification gap, as shown in Figure 1.

The secondary electrons are then collected by the pixelated Micromegas anode, which contains strips of pixels in the X and Y directions (pitch of 424.3 μm) with a total of 512 channels (256 on each axis) over an area of $10.8 \times 10.8 \text{ cm}^2$ [21], providing a 2D readout. A strip is fired either along the X or Y direction when the collected charge is higher than a preset threshold. It is sampled at 50 MHz (20 ns) by a self-triggered electronics system developed at LPSC [19]. The third spatial coordinate Z is provided by the combination of the known primary electron drift velocity and the timing sampling. The electronics is based on a specially designed 64 channel MIMAC ASIC [22] controlled by a data acquisition system [23].

The total ionization energy is measured by a charge pre-amplifier on the grid, by a Flash-ADC sampling also at 50 MHz. From the ionization energy value, it is possible to deduce the total recoil energy by taking into account the previously measured Ionization Quenching Factor (IQF) ([8] and [2]) corresponding to the fraction of the total kinetic energy released in ionization. This value depends on the nucleus, its kinetic energy, the gas mixture and gas pressure [19]. Existing models such as the Lindhard model [24], and existing Monte Carlo simulations do not seem to provide a good description of experimental results at energies below 60 keV [25]. That is why this IQF needs to be obtained experimentally for specifically defined configurations. IQF measurements for the MIMAC configuration were described in [26] and [25].

The aim of the ionization energy measurements and the 3D track reconstruction is to deduce the recoil kinetic energy and the direction of the initial scattered particle.

2.2 Low energy beam facilities: COMIMAC and LHI

In order to measure the IQF and evaluate the performances of one MIMAC chamber detector in terms of its angular resolution, we have performed experiments on both COMIMAC and LHI facilities.

COMIMAC is a table-top ion beam facility developed at LPSC [27]. It delivers a continuous beam of electrons and mono-charged calibrated ions with a kinetic energy ranging up to 50 keV. This facility is used to perform regular energy calibration using electrons and IQF measurements. COMIMAC uses a compacted 2.45 GHz (5W) Electron Cyclotron Resonance (ECR) source called COMIC [27]. A Wien filter is used to make a charge-to-mass ratio (q/m) separation of ions and allow for their selection. The filter is a combination of a 0.36 T magnetic field produced by permanent NdFeB magnets and a tunable 3.3 kV/cm electric field in a perpendicular configuration.

The LHI (Ligne expérimental à Haute Intensité) is an experimental ion beam line based on a 8.5 GHz ECR ion source coupled to a high resolution magnetic spectrometer. By applying a voltage on the plasma produced by the ECR ion source, the ions are extracted, collimated and sent to a high resolution magnetic spectrometer which separates the ion masses based on the q/m factor over a trajectory which is an arc of circle with a radius of $\rho = 0.7 \text{ m}$ with $B\rho$

= 0.23 T/m. The LHI beam line produces ions with well defined energies and uncertainties on the kinetic energy at the level of $\frac{\Delta E_{kin}}{E_{kin}} = 1\%$.

Both COMIMAC and LHI are coupled to the gas chamber via a 1 μm diameter hole that was made by a laser on a 13 μm thick stainless-steel foil. The hole interface coupled to a differential vacuum keeps a pressure independence between the beam line (10^{-5} mbar) and the ionization chamber (50 mbar). The ions are thus injected in the direction of the beam line parallel to the drift field in the chamber. We are exploring ways to make holes at an angle to the drift field for future measurements.

2.3 Experimental conditions

Different experiments performed on LHI or COMIMAC coupled to the MIMAC chamber assessed the influence of gas and detector purity, optimizing the chamber electric field value and homogeneity, amplification gap thickness, anode pixel efficiency and event selection algorithms. This has provided invaluable experience in evaluating the impact of different detector properties on its performance in terms of angular resolution.

The main experiment reported here was performed at LPSC using the LHI beam line with a 512 μm micromegas bulk gap detector. The MIMAC chamber employed was a $10.8 \times 10.8 \times 5 \text{ cm}^3$ single chamber. The grid voltage was set at -570 V and the cathode at -1320 V , while the anode was grounded. We also used a field cage in order to produce a uniform drift field. The LHI beam line facility delivered ions of kinetic energies between 5 keV and 25 keV. It was coupled to the MIMAC chamber from the cathode side and ions were injected in the drift (Z -axis) direction at an angle of $\theta = 0^\circ$ (same experimental configuration as [27], see Figure 3). The final ion kinetic energies inside the chamber had an additional component due to the voltage applied on the cathode (1.32 kV) in order to have the electronic board grounded.

After entering the chamber, the injected ions immediately interact with the gas atoms and the produced primary electrons drift to the micromesh. There the electrons enter the gap with an intense electric field producing the avalanches. Secondary electrons are created and collected by the pixelated anode readout.

3 Track Reconstruction

The secondary electrons created by the MIMAC Micromegas avalanche field reach the X and Y readout strips placed on the anode and provide the 2D positional information (Figure 2). The sampling of the anode every 20 ns allows the reconstruction of a 3D cloud of primary electrons for each detected event.

3.1 Track angle, angular resolution, depth and width definitions

One of the major challenges is to experimentally describe the 3D nuclear track in the active volume, since it is quite difficult to extract the information of the first collision between the injected ion and nuclei in the gas.

The ions delivered by LHI enter the chamber in the direction of the electron drift path along the Z -axis. We define the ion track depths as the projection of the primary electron cloud in the Z -direction:

$$z_{max} - z_{min} = (t_{max} - t_{min}) \times V_{drift}, \quad (3.1)$$

where V_{drift} is the electron drift velocity, and $t_{max} - t_{min}$ is the time difference between the first and last time signal of an ion event. The primary electron drift velocity was determined from MAGBOLTZ code [28] to be $V_{drift} = 22.9 \mu\text{m/ns}$ (for an applied electric field of 150 V/cm).

Another available observable is the track width (Figure 9b). We define it as the mean value of the number of strips triggered during a sampling interval on the X/Y readout.

The observed tracks are only a few mm long at such low energies. Figure 5 shows an example provided by the SRIM simulation for ^{19}F ions with kinetic energy of 6.3 keV and 26.3 keV, respectively.

The strategy for reconstructing a track direction is to perform a 3D linear regression fit on the pixelated electron cloud. Then we derive the direction of the fitted track with respect to the drift direction (Z -axis).

The 3D linear fit on pixelated primary electron clouds was performed by a least squares minimizing algorithm using the coordinate distances of the barycenters of each time-slice. An example of a 3D fit for a 26.32 keV (25 keV from the voltage acceleration plus 1.32 keV from the cathode voltage with respect to the ground) ^{19}F ion event (and a 2D representation of the same track) is shown in Figure 6. The combination of the straggling and the detector spatial resolution gives the direction of the recoil coming from $\hat{r}(\Omega)$ being interpreted as $\hat{r}'(\Omega')$, where $\Omega \equiv \Omega(\theta, \varphi)$ is the solid angle (Figure 3).

A polar angle θ was derived for each track, with 0° being the direction of the ^{19}F beam (Z -axis and primary electron drift direction). θ is actually the angular deviation from 0° from all effects combined, after the ion enters the chamber at 0° , hence its distribution can be used to define an angular resolution.

After an ionization occurs in the gas chamber, primary electrons have kinetic energies of the order of a few eV. This energy will quickly be lost because of multiple interactions with the gas molecules leading to thermalization and recombination [16]. By applying an electric field, the electrons drift towards the anode and their 3D Gaussian distribution $n(x, y, z; t)$ can be described as:

$$n(x, y, z; t) = \frac{n_0}{\sqrt{8\pi^3}} \times \frac{e^{-(x^2+y^2)/4D_t t}}{\sqrt{4D_t^2 t^2}} \times \frac{e^{-z^2/4D_l t}}{\sqrt{2D_l t}} \quad (3.2)$$

where D_t and D_l are the transverse (X/Y) and longitudinal (Z) diffusion coefficients, respectively.

Primary electrons experience transverse and longitudinal diffusion inside the gas chamber leading to longer and wider reconstructed track depths and widths, with the following standard deviations [29]:

$$\sigma_t = \tilde{D}_t \sqrt{L_d} \quad \text{and} \quad \sigma_l = \tilde{D}_l \sqrt{L_d}, \quad (3.3)$$

where L_d is the electron drift distance, and $\tilde{D}_{t/l} = \sqrt{2D_{t/l}/V_{drift}}$. For the MIMAC setup, we use for this paper, $L_d = 4.7$ cm.

\tilde{D}_t and \tilde{D}_l can be obtained with the MAGBOLTZ code. Diffusion depends on the type of gas and its pressure and on the drift electric field. At the drift electric field (150 V/cm) applied in the MIMAC chamber, the MAGBOLTZ simulation predicts the following transverse and longitudinal diffusion :

$$\begin{cases} \widetilde{D}_t = 253.1 \mu\text{m}/\sqrt{\text{cm}} \\ \widetilde{D}_l = 293.9 \mu\text{m}/\sqrt{\text{cm}} \end{cases} \quad (3.4)$$

giving a quasi-isotropic diffusion tensor.

3.2 Effects on angular resolution

The distribution of the reconstructed angle between the track and the low energy beam (denoted as θ) is not a Gaussian variable by definition. In contrast, θ_x and θ_y defined in Figure 3, appear as Gaussian variables in our experiments as shown in Figure 4. Both the distribution of the central ion entrance and the dispersion of the primary electron distribution contribute to the angular resolution:

- Distribution of the central ion entrance: The reconstructed direction deviates from the initial direction. This is due to several physical effects: (1) primary electron diffusion, (2) initial ion beam not exactly at zero degree: the hole through which the ions enter the chamber has a $1 \mu\text{m}$ diameter and $13 \mu\text{m}$ length (maximum angle of 4.4°) and (3) eventual bias from the reconstruction algorithm.
- Statistical dispersion: Spread of the distribution, usually defined as the standard deviation of a Gaussian Probability Distribution Function (PDF). The main contribution to the statistical dispersion should be the straggling of ions, which is a convolution of multiple small angle scattering with the nuclei of the gas. Other factors deteriorating angular resolution are the interactions of the primary electrons inside the gas chamber - straggling caused by electron collisions and re-combinations with the gas atoms [17], and diffusion [30].

The measured distribution of the central ion entrance is small ($< 1^\circ$) and the dispersion has an effect about 10 times larger than the central shift (more than 4 times for 26.3 keV), as shown in Table 1. Thus we simply take the spread of the distribution as the definition of angular resolution.

| Data Label (keV) | 6.3 | 9.3 | 11.3 | 13.8 | 16.3 | 18.8 | 21.3 | 23.8 | 26.3 |
|---------------------------|-------|------|------|------|------|------|------|-------|------|
| $\hat{\mu}_{\theta_x}$ | 0.7 | 0.24 | 0.08 | 0.08 | 0.21 | 0.29 | 0.24 | 0.29 | 0.44 |
| $\hat{\sigma}_{\theta_x}$ | 13.28 | 7.14 | 4.75 | 3.56 | 2.79 | 2.53 | 2.18 | 2.06 | 1.91 |
| $\hat{\mu}_{\theta_y}$ | 0.96 | 0.92 | 0.5 | 0.28 | 0.29 | 0.07 | 0.05 | -0.05 | 0.17 |
| $\hat{\sigma}_{\theta_y}$ | 14.17 | 6.93 | 4.49 | 3.34 | 2.65 | 2.33 | 2.01 | 1.84 | 1.71 |

Table 1. Gaussian fit parameters of θ_x and θ_y distributions for different kinetic energy ^{19}F ion events.

3.3 Analysis results on track depth, width and angular resolution

The analysis was performed for ^{19}F ions with kinetic energies of 6.3 keV, 9.3 keV, 11.3 keV, 13.8 keV, 16.3 keV, 18.8 keV, 21.3 keV, 23.8 keV and 26.3 keV and with more than 1.8×10^4 final events for each energy. Figure 6 and Figure 7 show examples of track trajectories in ZX , ZY projections and in 3D for ions with kinetic energies of 26.3 keV and 9.3 keV, respectively.

The reconstructed average track depths and widths are shown in Figure 9, as a function of ion kinetic energies. For the lowest ion kinetic energy of 6.3 keV, a track of about 3 mm depth and 1.5 mm wide was measured. At the kinetic energy of 26.3 keV, the ion tracks are showing a depth longer than 7 mm, with an average width of 2.8 mm.

The final reconstructed angle as a function of the ion kinetic energy is shown in Figure 8. Its dispersion is better than the required 20° [2] even at the lowest kinetic energy of 6.3 keV.

The derived uncertainty on angular resolution $\Delta\theta$ is based on the determination of the spatial coordinates of the reconstructed primary electron cloud and the error of the 3D linear fit:

$$\begin{aligned}\Delta\theta(x, y, z)\Big|_{\theta=\bar{\theta}} &= \sqrt{\left(\frac{\partial\theta}{\partial x}\right)^2\Delta^2(x) + \left(\frac{\partial\theta}{\partial y}\right)^2\Delta^2(y) + \left(\frac{\partial\theta}{\partial z}\right)^2\Delta^2(z) + \Delta_{\text{fit}}^2} \\ &\simeq \frac{\cos^2\theta}{z}\sqrt{\Delta_{XY}^2 + \tan^2\theta \cdot \Delta^2(z)}\end{aligned}\quad (3.5)$$

where $\Delta(z) = \Delta(V_{\text{drift}} \cdot t)$ mainly depends on sampling time, $\Delta_{XY} = \Delta(x) = \Delta(y)$ is the intrinsic systematic uncertainty due to alignment and finite size of anode strips (Figure 2). The fit error Δ_{fit} is negligible, so we can only take the first term into consideration. For $\theta \approx 0^\circ$ case, the uncertainty can be further approximated and simplified to be only dependent on the pitch of the anode strips and the reconstructed track length:

$$\Delta\theta(x, y, z)\Big|_{\theta=\bar{\theta}\approx 0^\circ} = \frac{\Delta_{XY}}{L}, \quad (3.6)$$

where Δ_{XY} is the same as in (3.5) and L describes the primary electron cloud dimensions (the reconstructed ion track length). The error we obtained is $\pm 1.1^\circ$ for the lowest ion kinetic energy and $\pm 0.45^\circ$ for the highest.

We have applied various algorithms in order to find the best way to reconstruct the initial angle. The differences among these algorithms are mainly whether to use the entire electron cloud or only part of it, and how to set weight on each pixel. Modifying the algorithms to use only the first part of the track (with a χ^2 test to select the optimum number of points) did not yield an improvement on the angular resolution. In addition, initial and final time slices of the track usually have a larger than average deviation from the track direction. This is because the anode samples the endpoints of the transversely diffused primary electron cloud. Removing the first and last time slice does not produce better results either.

We finally chose to use the barycenter weighted method with the information from all 3D pixels, which average reconstructed angle is closest to the initial 0° angle, and has the lowest dispersion.

4 Simulations and Measurements

Nuclear ^{19}F track depth and width measurements have been compared to the simulations performed with the SRIM (Stopping and Range of Ions in Matter) code, a software allowing to calculate interactions of ions with matter ([31] and [32]).

It is based on a Monte Carlo simulation method, using the binary collision approximation with a random selection of the impact parameter of the next colliding ion. The inputs of SRIM include the type and initial energy of the ion, as well as the target definition and density. With these information, SRIM computes the three-dimensional distribution of the

ions in the target and its parameters, such as penetration depth, its spread along the ion beam and perpendicular to it (called straggling); all target atom cascades in the target are followed in detail. But the effects of drift and diffusion in the electric field of the chambers are not taken into account.

To estimate the diffusion effects due to the drift, we use the diffusion parameters computed by MAGBOLTZ. Billard et al.[33] has shown that MAGBOLTZ estimates for the primary electron velocity are similar to the measured ones in a pure CF_4 gas at 50 mbar. Couturier et al.[34] has reported measurements performed by the MIMAC team with the same gas and pressure. In Figure 9b, we show experimental width results compared to SRIM + MAGBOLTZ simulations, while the left hand side of the figure (Figure 9a) shows the depth. Although the SRIM outputs are in agreement with experimental tracks for MeV range kinetic energies, the measured track depths that we observe are much longer than the simulated ones, in the ion kinetic energy range of 6-26 keV. The measured track widths also larger than the SRIM + MAGBOLTZ diffusion expectations, but the differences are not as important.

We define k_{trans} as the ratio between the measured transverse diffusion to the predicted MAGBOLTZ transverse diffusion. Assuming the ratio of longitudinal to transverse diffusion computed by MAGBOLTZ does not change, we expect a measured longitudinal diffusion defined as $k_{trans} \cdot D_l$ (purple triangles in Figure 9a). There is still a large difference between observed and simulated depths.

In Figure 9a, we also show an extreme case for SRIM simulation which includes 3 times the longitudinal diffusion computed by MAGBOLTZ.

Systematic effects, such as the detector anode strips having a lack of efficiency, and the dilution of the electron cloud, lead to some non detections of parts of the tracks, which would result in shorter measured tracks but not longer tracks compared to the ones predicted by SRIM + MAGBOLTZ.

The only effect that we could think of, which would increase the average track lengths is the selection bias in the analysis, we request more than 2 pixels. The number of pixels triggered for each energy is however larger, only at the lowest energy of 6 keV (see Figure 10), could we expect some bias.

Understanding and improving the simulations to reproduce measurements presented here is an important task for the future.

5 Conclusion

Having a good estimate of the initial direction of nuclear recoils is a key issue for directional Dark Matter detectors. This work shows an experimental study of the main parameters involved in the 3D low energy nuclear recoil track measurements.

MIMAC is currently the only directional Dark Matter detector whose prototype is able to display 3D tracks of nuclear recoils down to an energy level of ≈ 5 keV and track length of a few mm. The $10.8 \times 10.8 \times 5$ cm³ prototype used in this experiment shows good results in terms of angular resolution of ion detection - using the LHI beamline as ion source set at 0° in the direction perpendicular to the cathode. For ^{19}F ion kinetic energies between 6.3 keV and 26.3 keV, the angular resolution, ranges between 14° and 2° , respectively, which is much better than required.

We are studying techniques to drill holes at an angle to the drift direction, in order to measure ion tracks at non-zero angles to the drift direction. We are also currently analysing data from a $(10 \times 10 \times 25)$ cm³ MIMAC chamber which detects 565 keV neutrons produced by protons of 2.3 MeV on a ⁷Li target in an experiment performed at the AMANDE facility [35] at Cadarache (France). In the data sample, nuclear recoils with different angles to the drift direction have been produced. The results will be discussed in a forthcoming paper.

The main uncertainty contributions to the angular resolution are from straggling, anode pixelization and diffusion. Experimentally obtained track depths have been compared to Monte Carlo SRIM simulations and are significantly longer than expected in the keV energy range. Not everything is well understood at these low energies, and more work is also needed on the simulation side. Experimental measurements like the ones we are presenting in this paper are fundamental.

The quality of the track reconstruction with the MIMAC detector presented in this study is very encouraging. It is an important step showing the experimental feasibility to access the Galactic origin of a low energy nuclear recoil produced by an elastic WIMP collision.

References

- [1] D. N. Spergel, *Motion of the Earth and the detection of weakly interacting massive particles*, *Physical Review D* **37** (1988) 1353.
- [2] J. Billard, F. Mayet and D. Santos, *Assessing the discovery potential of directional detection of dark matter*, *Physical Review D - Particles, Fields, Gravitation and Cosmology* **85** (2012) 35006 [1110.6079].
- [3] M. W. Goodman and E. Witten, *Detectability of certain dark-matter candidates*, *Physical Review D* **31** (1985) 3059.
- [4] C. Couturier, J. P. Zopounidis, N. Sauzet, F. Naraghi and D. Santos, *Dark matter directional detection: comparison of the track direction determination*, *Journal of Cosmology and Astroparticle Physics* **2017** (2017) 27.
- [5] J. B. R. Battat, J. Brack, E. Daw, A. Dorofeev, A. C. Ezeribe, J.-L. Gauvreau et al., *First background-free limit from a directional dark matter experiment: Results from a fully fiducialised DRIFT detector*, *Physics of the Dark Universe* **9-10** (2015) 1.
- [6] C. Deaconu, M. Leyton, R. Corliss, G. Druitt, R. Eggleston, N. Guerrero et al., *Measurement of the directional sensitivity of Dark Matter Time Projection Chamber detectors*, *Physical Review D* **95** (2017) 122002 [1705.05965].
- [7] K. Nakamura, K. Miuchi, T. Tanimori, H. Kubo, H. Nishimura, J. D. Parker et al., *NEWAGE - Direction-sensitive Dark Matter Search Experiment*, *Physics Procedia* **61** (2015) 737.
- [8] D. Santos, G. Bosson, J. L. Bouly, O. Bourrion, C. Fourel, O. Guillaudin et al., *MIMAC: Micro-tpc MAtrix of chambers for dark matter directional detection*, *Journal of Physics: Conference Series* **469** (2013) 12014 [1311.0616].
- [9] F. Mayet, A. M. Green, J. B. R. Battat, J. Billard, N. Bozorgnia, G. B. Gelmini et al., *A review of the discovery reach of directional Dark Matter detection*, **1602.03781**.
- [10] S. Ahlen, N. Afshordi, J. B. R. Battat, J. Billard, N. Bozorgnia, S. Burgos et al., *The case for a directional dark matter detector and the status of current experimental efforts*, *International Journal of Modern Physics A* **25** (2009) 1 [0911.0323].
- [11] J. B. R. Battat, I. G. Irastorza, A. Aleksandrov, T. Asada, E. Baracchini, J. Billard et al., *Readout technologies for directional WIMP Dark Matter detection*, *Physics Reports* **662** (2016) 1.

- [12] J. Billard, E. Figueroa-Feliciano and L. Strigari, *Implication of neutrino backgrounds on the reach of next generation dark matter direct detection experiments*, *Physical Review D - Particles, Fields, Gravitation and Cosmology* **89** (2014) [[1307.5458](#)].
- [13] J. Billard, F. Mayet and D. Santos, *Exclusion limits from data of directional dark matter detectors*, *Physical Review D - Particles, Fields, Gravitation and Cosmology* **82** (2010) 1 [[arXiv:1006.3513v1](#)].
- [14] C. Amole, M. Ardid, I. J. Arnquist, D. M. Asner, D. Baxter, E. Behnke et al., *Dark Matter Search Results from the PICO – 60 C₃F₈ Bubble Chamber*, *Physical Review Letters* **118** (2017) 251301.
- [15] J. Billard, F. Mayet, J. F. Macías-Pérez and D. Santos, *Directional detection as a strategy to discover Galactic Dark Matter*, *Physics Letters B* **691** (2010) 156.
- [16] F. Sauli, *Principles of operation of multiwire proportional and drift chambers*. 1991. 79-188. CERN, 1991.
- [17] J. Billard, F. Mayet, D. Santos, F. Mayet, D. Santos, S. F. Biagi et al., *Track reconstruction with MIMAC*, *EAS Publications Series* **53** (2012) 137.
- [18] Q. Riffard, D. Santos, O. Guillaudin, G. Bosson, O. Bourrion, J. Bouvier et al., *MIMAC low energy electron-recoil discrimination measured with fast neutrons*, *Journal of Instrumentation* **11** (2016) P08011 [[1602.01738](#)].
- [19] C. Couturier, O. Guillaudin, F. Naraghi, Q. Riffard, D. Santos, N. Sauzet et al., *Directional detection of Dark Matter with the MICRO-tpc MATRIX of Chambers*, [1607.08765](#).
- [20] I. Giomataris, R. De Oliveira, S. Andriamonje, S. Aune, G. Charpak, P. Colas et al., *Micromegas in a bulk*, *Nuclear Instruments and Methods in Physics Research Section A: Accelerators, Spectrometers, Detectors and Associated Equipment* **560** (2006) 405.
- [21] F. J. Iguaz, D. Attié, D. Calvet, P. Colas, F. Druillolle, E. Ferrer-Ribas et al., *Micromegas detector developments for Dark Matter directional detection with MIMAC*, *Journal of Instrumentation* **6** (2011) P07002.
- [22] J. P. Richer, O. Bourrion, G. Bosson, O. Guillaudin, F. Mayet, D. Santos et al., *Development and validation of a 64 channel front end ASIC for 3D directional detection for MIMAC*, *Journal of Instrumentation* **6** (2011) C11016.
- [23] O. Bourrion, G. Bosson, C. Grignon, J. L. Bouly, J. P. Richer, O. Guillaudin et al., *Data acquisition electronics and reconstruction software for real time 3D track reconstruction within the MIMAC project*, *Journal of Instrumentation* **6** (2011) C11003 [[1110.4348](#)].
- [24] J. Lindhard, V. Nielsen, M. Scharff and P. V. Thomsen, *Integral equations governing radiation effects. (Notes on atomic collisions, III)*, *Kgl. Danske Videnskab. Selskab Mat.-fys. Medd.* **33** (1963) 1.
- [25] Q. Riffard, *To cite this version : Détection directionnelle de matière sombre avec MIMAC*, Ph.D. thesis, Université of Grenoble, 2016.
- [26] O. Guillaudin, J. Billard, G. Bosson, O. Bourrion, T. Lamy, F. Mayet et al., *Quenching factor measurement in low pressure gas detector for directional dark matter search*, *EAS Publications Series* **53** (2012) 119 [[1110.2042](#)].
- [27] J. F. Muraz, J. Médard, C. Couturier, C. Fourrel, O. Guillaudin, T. Lamy et al., *A table-top ion and electron beam facility for ionization quenching measurement and gas detector calibration*, *Nuclear Instruments and Methods in Physics Research, Section A: Accelerators, Spectrometers, Detectors and Associated Equipment* **832** (2016) 214.
- [28] S. F. Biagi, *Monte Carlo simulation of electron drift and diffusion in counting gases under the influence of electric and magnetic fields*, *Nuclear Instruments and Methods in Physics Research Section A: Accelerators, Spectrometers, Detectors and Associated Equipment* **421** (1999) 234.

- [29] J. Billard, *Détection directionnelle de matière sombre avec MIMAC*, Ph.D. thesis, Université of Grenoble, 2012.
- [30] A. Peisert and F. Sauli, *Drift and Diffusion of Electrons in Gases: A Compilation (With an Introduction to the Use of Computing Programs)*, tech. rep., CERN-84-08, 1984.
- [31] J. F. Ziegler, M. D. Ziegler and J. P. Biersack, *SRIM - The stopping and range of ions in matter (2010)*, *Nuclear Instruments and Methods in Physics Research, Section B: Beam Interactions with Materials and Atoms* **268** (2010) 1818.
- [32] S. Agostinelli, J. Allison, K. Amako, J. Apostolakis, H. Araujo, P. Arce et al., *Geant4—a simulation toolkit*, *Nuclear Instruments and Methods in Physics Research Section A: Accelerators, Spectrometers, Detectors and Associated Equipment* **506** (2003) 250.
- [33] J. Billard, F. Mayet, G. Bosson, O. Bourrion, O. Guillaudin, J. Lamblin et al., *In situ measurement of the electron drift velocity for upcoming directional Dark Matter detectors*, *Jinst* **9** (2014) P01013 [1305.2360].
- [34] C. Couturier, Q. Riffard, N. Sauzet, O. Guillaudin, F. Naraghi and D. Santos, *Cathode signal in a TPC directional detector: implementation and validation measuring the drift velocity*, *Journal of Instrumentation* **12** (2017) P11020.
- [35] V. Gressier, J. F. Guerre-Chaley, V. Lacoste, L. Lebreton, G. Pelcot, J. L. Pochat et al., *AMANDE: a new facility for monoenergetic neutron fields production between 2 keV and 20 MeV*, *Radiation Protection Dosimetry* **110** (2004) 49.

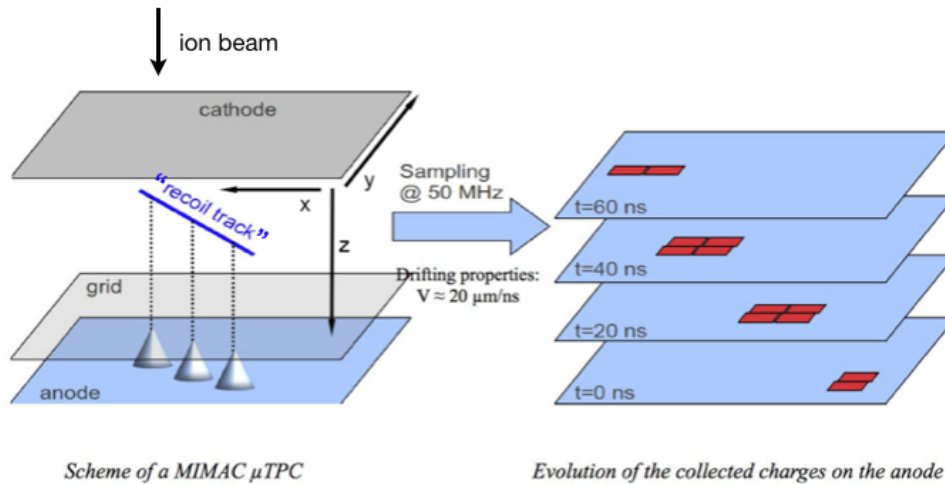


Figure 1. A simple scheme of a MIMAC detector chamber (left) and an example how sampling at 50 MHz is performed (right). This configuration allows us to determine a 3D cloud of primary electrons and reconstruct the ion track. The amplification gap in this experiment is $512 \mu\text{m}$ with an electric field of over 11 kV/cm .

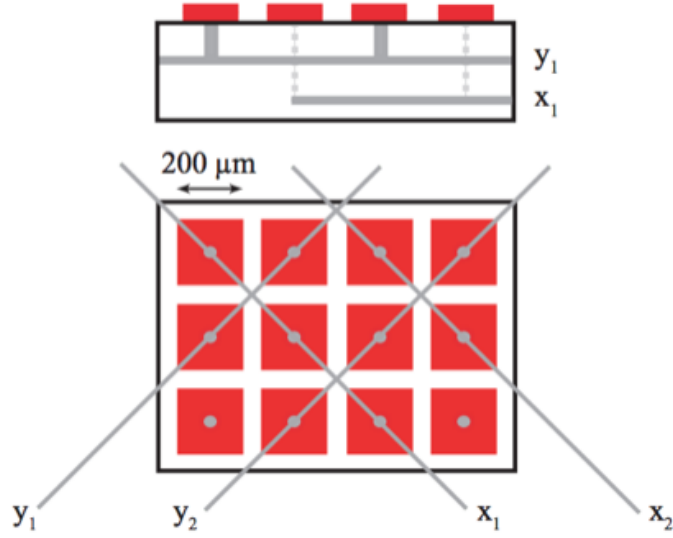


Figure 2. Readout electrode placed on the anode is segmented in X and Y direction strips providing 2D positional information for each event.

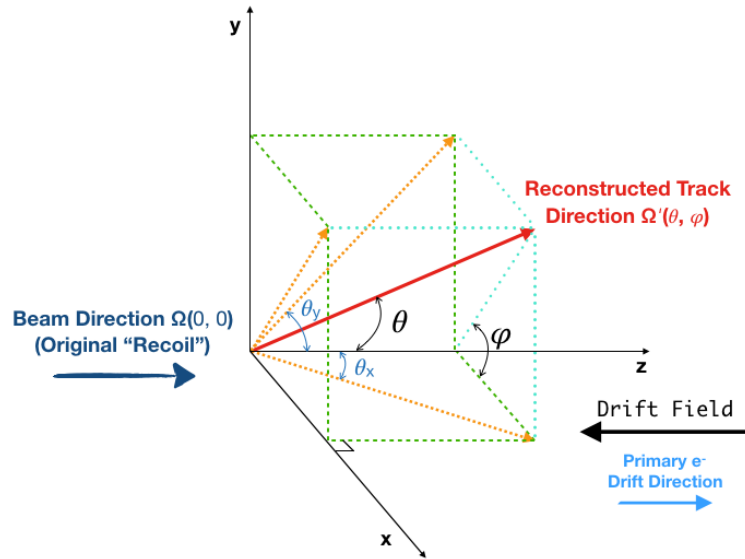


Figure 3. Schematic diagram for geometrical observables in 3D space. The incoming beam direction is along the Z -axis, which is the same as the direction of the electric drift field. An example of reconstructed track direction $\Omega(\theta, \varphi)$ is shown as a red arrow with polar angle θ and azimuthal angle φ indications. The orange arrows represent the 2D projections of this 3D directional vector, defining θ_x and θ_y .

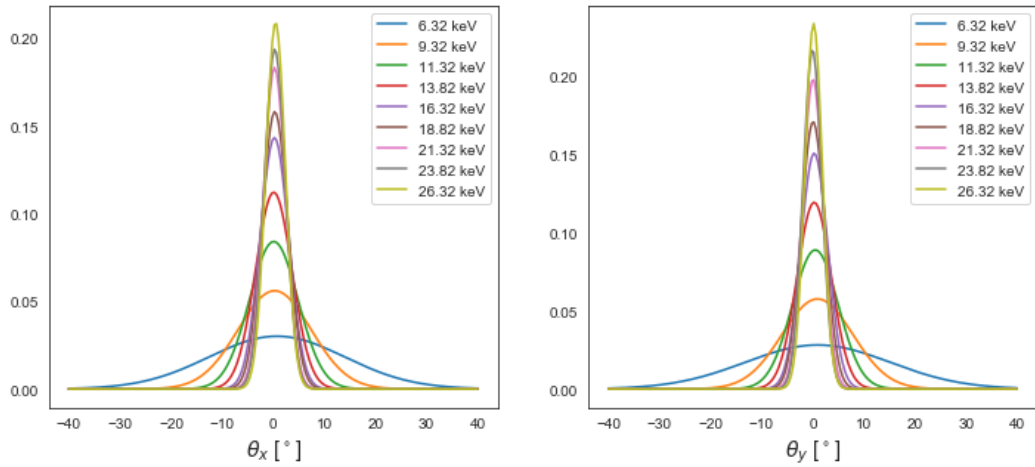


Figure 4. Normalized distributions of θ_x and θ_y for ^{19}F ions of kinetic energy ranging from 6.3 keV to 26.3 keV.

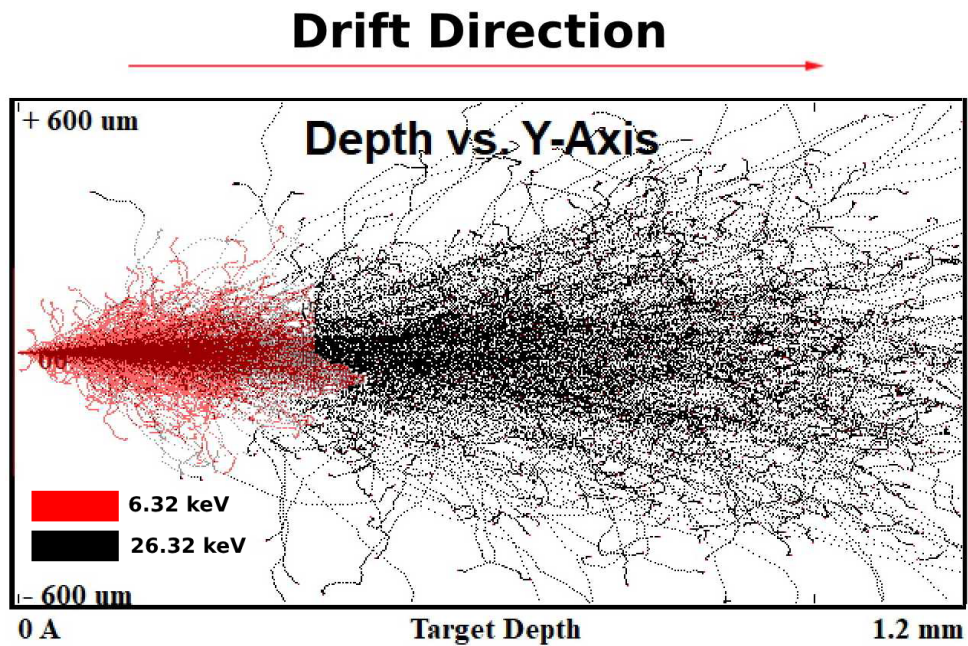


Figure 5. Scattering is the dominant contribution to our angular resolution. Taken from a SRIM simulation, this image shows how an ion path is deviated due to interactions with gas for ions of kinetic energy of 6.32 keV (in red) and 26.32 keV (in black). The left vertical axis shows the position of the cathode, while the horizontal axis is the ion track depth (same as Z-axis in Figure 3). The red arrow shows the drift direction of primary electrons. The detected cloud of primary electrons therefore reflects not only the limitation of the detector to discern the initial track direction, but mostly the non-linear energy loss and multiple small-angle scattering of ions.

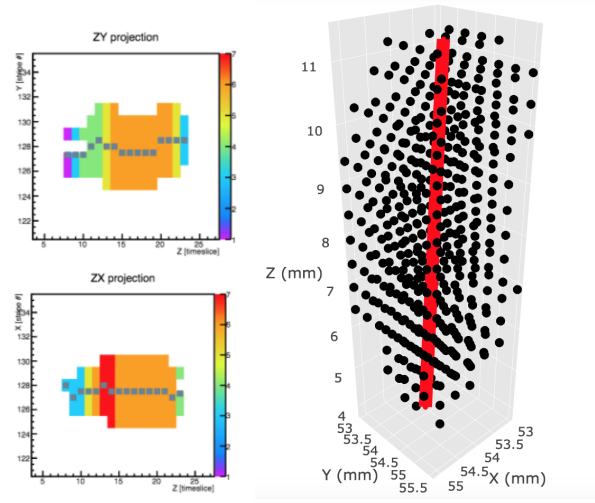


Figure 6. Example of an ion track in ZX and ZY projection using barycenter representation (left) and 3D (right) for an ion of kinetic energy of 26.3 keV. To derive the direction of the track, a 3D linear fit is performed on the 3D cloud of primary electrons.

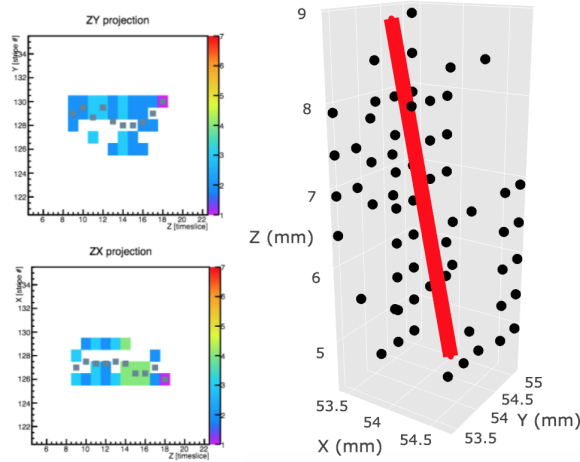


Figure 7. Example of an ion track in ZX and ZY projection using barycenter representation (left) and 3D (right) for an ion of kinetic energy of 9.3 keV. To derive the direction of the track, a 3D linear fit is performed on the 3D cloud of primary electrons.

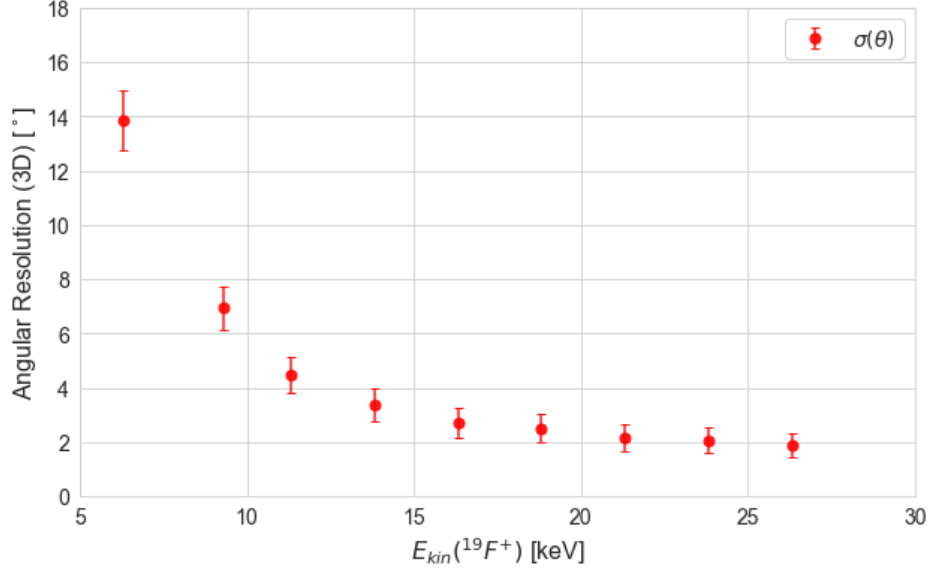


Figure 8. MIMAC angular resolution as a function of ${}^{19}\text{F}$ ion kinetic energy. At lower energies, the ion tracks are shorter and have more straggling resulting in worse angular resolution and bigger error bars. The angular resolution is better than 20° down to a kinetic energy of 6.3 keV, and is below 10° for a kinetic energy of 9.3 keV. Error bars are derived from the pixel strips pitch and reconstructed track length as described in the text.

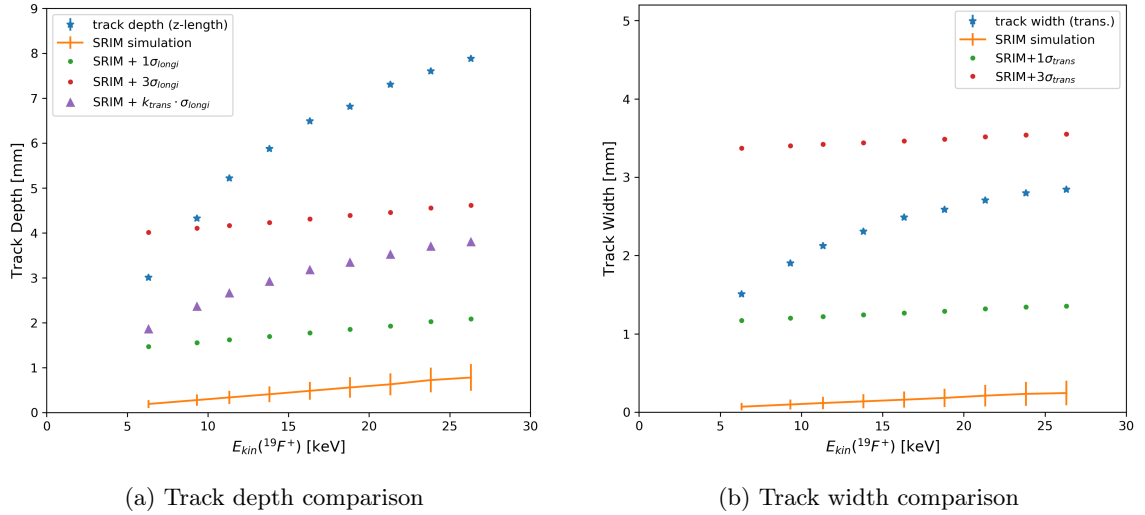


Figure 9. Comparison of ion track depths and widths at different energies between experiment (blue stars) and simulation using SRIM and MAGBOLTZ (orange curve for SRIM-only, green when the diffusion as computed by MAGBOLTZ is added, red in an extreme case of adding 3 times the MAGBOLTZ computed diffusion). Left: Track depths comparison. We also show "SRIM + $k_{trans} \cdot D_l$ of MAGBOLTZ" in this subplot, where k_{trans} depends on energy and is derived from the width result. Right: Track widths comparison.

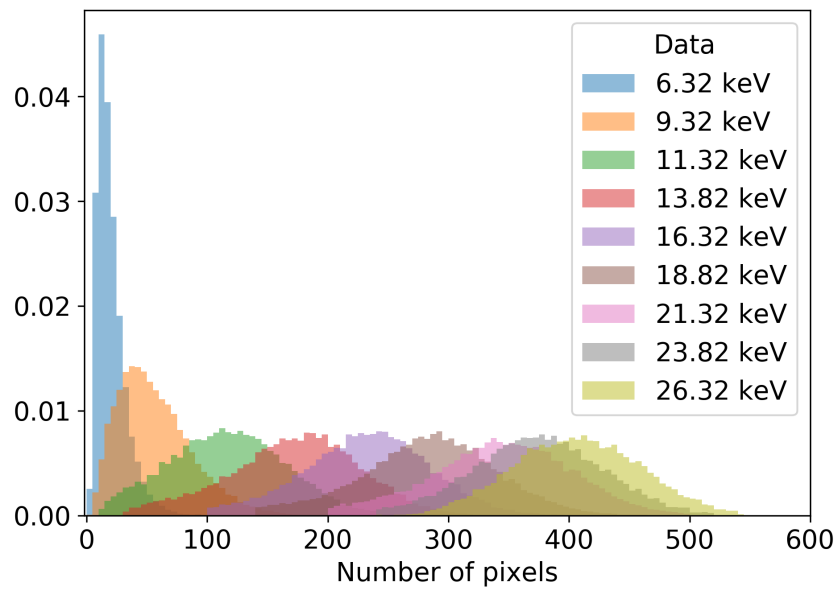


Figure 10. The number of pixels triggered for each kinetic energy of ^{19}F ion.